



## OPEN

SUBJECT AREAS:  
ENZYME MECHANISMS  
BIOENERGETICSReceived  
5 December 2013Accepted  
9 June 2014Published  
26 June 2014

## Dark-operative protochlorophyllide oxidoreductase generates substrate radicals by an iron-sulphur cluster in bacteriochlorophyll biosynthesis

Jiro Nomata<sup>1\*</sup>, Toru Kondo<sup>2†</sup>, Tadashi Mizoguchi<sup>3</sup>, Hitoshi Tamiaki<sup>3</sup>, Shigeru Itoh<sup>2‡</sup> & Yuichi Fujita<sup>1</sup><sup>1</sup>Graduate School of Bioagricultural Sciences, Nagoya University, Furo-cho, Chikusa-ku, Nagoya 464-8601, Japan, <sup>2</sup>Graduate School of Science, Nagoya University, Furo-cho, Chikusa-ku, Nagoya 464-8602, Japan, <sup>3</sup>Graduate School of Life Sciences, Ritsumeikan University, Kusatsu, Shiga 525-8577, Japan.

Correspondence and requests for materials should be addressed to Y.F. (fujita@agr.nagoya-u.ac.jp)

\* Current address: Chemical Resources Laboratory, Tokyo Institute of Technology, Nagatsuta, 4259, Midori-ku, Yokohama, 226-8503.

† Current address: Department of Physics, Tokyo Institute of Technology, Ookayama, Meguro-ku, Tokyo 152-8551, Japan.

‡ Current address: Centre for Gene Research, Nagoya University, Furo-cho, Chikusa-ku, Nagoya 464-8602, Japan.

Photosynthesis converts solar energy to chemical energy using chlorophylls (Chls). In a late stage of biosynthesis of Chls, dark-operative protochlorophyllide (Pchlde) oxidoreductase (DPOR), a nitrogenase-like enzyme, reduces the C17=C18 double bond of Pchlde and drastically changes the spectral properties suitable for photosynthesis forming the parental chlorin ring for Chl *a*. We previously proposed that the spatial arrangement of the proton donors determines the stereospecificity of the Pchlde reduction based on the recently resolved structure of the DPOR catalytic component, NB-protein. However, it was not clear how the two-electron and two-proton transfer events are coordinated in the reaction. In this study, we demonstrate that DPOR initiates a single electron transfer reaction from a [4Fe-4S]-cluster (NB-cluster) to Pchlde, generating Pchlde anion radicals followed by a single proton transfer, and then, further electron/proton transfer steps transform the anion radicals into chlorophyllide (Chlide). Thus, DPOR is a unique iron-sulphur enzyme to form substrate radicals followed by sequential proton- and electron-transfer steps with the protein folding very similar to that of nitrogenase. This novel radical-mediated reaction supports the biosynthesis of Chl in a wide variety of photosynthetic organisms.

In Chl biosynthesis, Pchlde reduction is the final reaction forming the conjugated  $\pi$ -system, the chlorin structure of Chl *a*, by the stereo-specific reduction of the C17=C18 double bond (Fig. 1a). There are two evolutionary unrelated Pchlde reductases, one is the light-dependent Pchlde oxidoreductase (LPOR)<sup>1</sup>, which requires light for catalysis, and the other is DPOR<sup>2</sup>, which operates in a light-independent manner.

LPOR is composed of a single polypeptide that belongs to short-chain dehydrogenase/reductase (SDR) family. LPOR is the responsible enzyme for light-dependent greening of angiosperms because LPOR operates as the sole Pchlde reductase in angiosperms<sup>1</sup>. Since the LPOR reaction is triggered by light, this enzyme provides a unique opportunity to study the reactions by ultrafast timescale. Although crystal structure of LPOR has not yet been revealed, several spectroscopic reaction intermediates were detected by triggering the reaction with a short laser pulse allowing to elucidate the catalytic cycle of LPOR<sup>3,4</sup>. These kinetic analyses suggested that a hydride transfer from NADPH to C18 is induced by light activation of Pchlde followed by several light-independent reactions including a proton transfer from a Tyr residue to C17, release of Chlide and exchange of cofactors<sup>5</sup>.

In oxygenic photosynthetic organisms except for angiosperms, DPOR serves as the determinant enzyme mediating the greening in the dark. Anoxygenic photosynthetic bacteria employ DPOR as the sole Pchlde reductase in bacteriochlorophyll biosynthesis. DPOR consists of two separable components, L-protein (a BchL homodimer) and NB-protein (a BchN-BchB heterotetramer), which are structurally related to Fe protein (a NifH homodimer) and MoFe protein (a NifD-NifK heterotetramer) of nitrogenase, respectively. Similar to nitrogenase, L-protein is the ATP-dependent reductase component<sup>6</sup> for the catalytic component, NB-protein, where Pchlde reduction takes place<sup>7</sup>. A reaction cycle of L-protein was proposed based on analysis with a site-directed L-protein variant and an ATPase inhibitor<sup>8</sup>. Furthermore, using a new specific inhibitor nicotinamide (NA), a reaction cycle of NB-protein was also proposed to consist of 10 steps<sup>9</sup> as follows: 1) the oxidized NB-protein binds to Pchlde; 2) the reduced L-protein (that is reduced by ferredoxin<sup>10</sup>) binds to the NB-protein–Pchlde complex; 3) an electron is

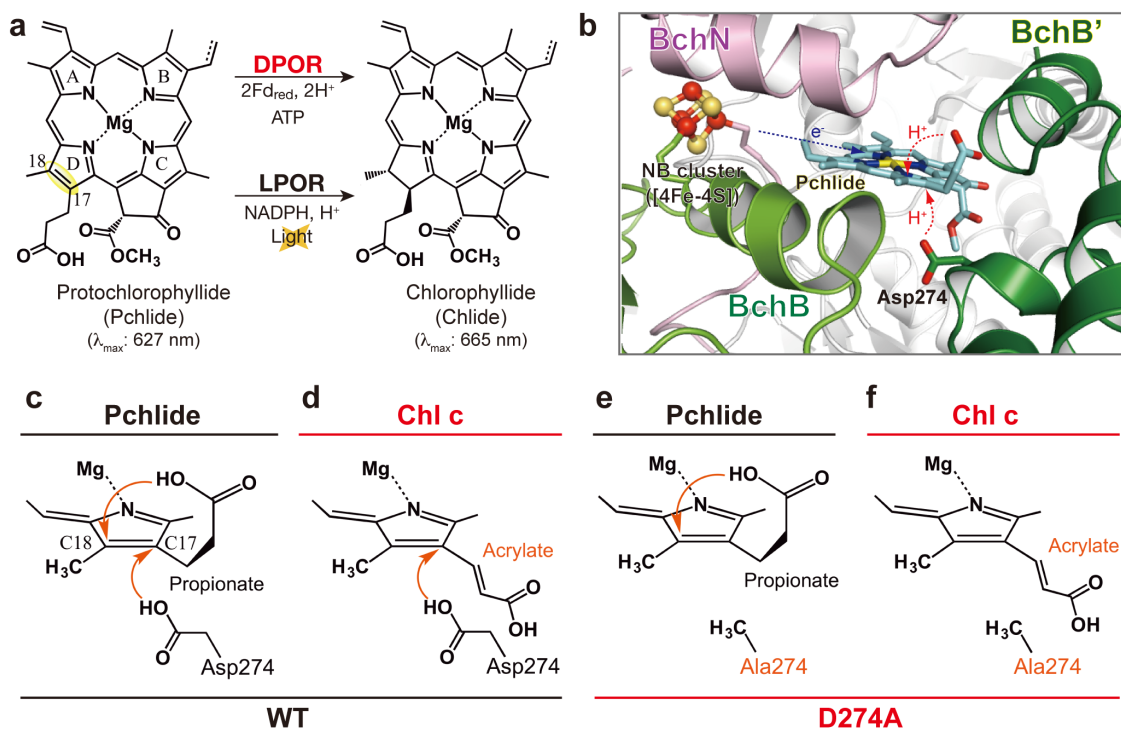


**Figure 1** | (a) Pchlide reduction. The C17 = C18 double bond of Pchlide D-ring (yellow) is *trans*-reduced by DPOR (upper) and LPOR (lower) to form Chlide. (b) Close-up view of the catalytic site of NB-protein. The direct electron transfer from the NB-cluster to Pchlide is shown by a dashed blue arrow. The proton transfers from BchB'-Asp274 and the propionate to Pchlide are shown by dashed red arrows. (c–f) Schematic representation of the combination of WT-D274A NB-protein, and Pchlide-Chl *c*; the native combination (c), WT NB-protein and Chl *c* (d), D274A NB-protein and Pchlide (e) and D274A NB-protein and Chl *c* (f).

transferred to the NB-cluster (that is coupled with ATP hydrolysis by the L-protein); 4) the oxidized L-protein is released from the NB-protein; 5) Pchlide is reduced by the single electron from the NB-cluster; 6) the second reduced L-protein binds to the NB-protein; 7) the NB-cluster is reduced again by the second L-protein; 8) Pchlide reduction is completed by the second electron transfer from the NB-cluster; 9) the oxidized L-protein is released; and 10) Chlide is released.

Crystal structures of individual DPOR components and a hexameric L-protein–NB-protein complex were recently revealed<sup>11–14</sup>. Then, DPOR became the first enzyme whose reaction mechanism was proposed on the basis of crystal structures among enzymes of the Mg branch. In our previous study<sup>12</sup>, we proposed a molecular basis for the stereospecificity of the C17=C18 reduction based on the crystal structure of the NB-protein isolated from the purple bacterium *Rhodospirillum rubrum* (Fig. 1b). The model predicted that Asp274 in BchB' and a propionate group at C17 of the substrate donate protons to C17 and C18, respectively (Fig. 1b, c). In this reaction, two electron transfer events from the NB-cluster to Pchlide (steps 5 and 8 mentioned above) are accompanied with two proton transfer events. Considering that the NB-cluster, a [4Fe-4S] cluster, delivers directly one electron at a time to Pchlide, the reaction intermediates must include Pchlide radicals. However, such reaction intermediates including Pchlide radicals have never been detected so far and it remained unclear how these electron and proton transfer events are coordinated.

Radical enzymes catalyse a variety of reactions that are chemically difficult to achieve. Most radical enzymes, including ribonucleotide reductases<sup>15</sup>, vitamin B<sub>12</sub>-dependent enzymes<sup>16</sup> and radical-SAM enzymes<sup>17</sup>, generate cofactor radicals. For example, vitamin B<sub>12</sub>-dependent and radical SAM enzymes generate a 5'-deoxyadenosyl radical, and ribonucleotide reductases generate a thiyl radical to induce the abstraction of a hydrogen atom from the 3' carbon of ribonucleotide phosphate. In contrast, enzymes generating substrate

radicals by direct electron transfer are limited. Recently, 2-hydroxyisocaproyl-CoA dehydratase (2HCD) from a strict anaerobe *Clostridium difficile* has been demonstrated that a substrate radical (ketyl radical) is generated by electron transfer from a [4Fe-4S] cluster to induce a dehydration reaction<sup>18</sup>. 2HCD represents a novel class of radical enzymes.

Here we show that DPOR is another unique radical enzyme generating substrate (Pchlide) radicals by a [4Fe-4S] cluster in NB-protein and propose a reaction scheme, in which Pchlide radicals are converted to the product Chlide by a second reduction with the [4Fe-4S] cluster. This radical mediated Pchlide reduction mechanism by DPOR appears to be distributed among not only anoxygenic photosynthetic bacteria but also oxygenic phototrophs including cyanobacteria, green algae and lower land plants.

## Results

In the DPOR assay system in this study, a stable substrate-bound catalytic component, Pchlide-bound NB-protein, was prepared and pre-incubated with L-protein, dithionite and an ATP-regeneration system<sup>7</sup>. The reactions were initiated by the addition of ATP and monitored by absorption and electron paramagnetic resonance (EPR) spectroscopy. Absorption spectra were measured at 5 °C to facilitate the detection of intermediates by slowing down the whole reaction process. If Pchlide radicals are generated during the reaction, they can be detected directly by monitoring absorbance changes or by EPR after rapid freezing of samples. Using the wild-type (WT) Pchlide-bound NB-protein, only the absorption spectrum indicating Chlide formation was detected 30 s after the reaction without any intermediate spectra showing catalytic intermediates (Fig. S1 and inset). The prediction of proton donors from the crystal structure of NB-protein allows us to use a substrate analog Chl *c* and a site-directed variant to trap reaction intermediates by blocking the proton donor processes. We examined combinations of Chl *c* that has



C17-acrylate instead of C17-propionate and a NB-protein variant D274A that has a site-directed BchB variant with Ala274 instead of Asp274 (Figs. 1d–f).

It is expected that the proton transfer is completely blocked in a combination of D274A and Chl *c* (Figs. 1f and 2a). Upon the addition of ATP, the absorption peaks were decreased slowly with a time constant ( $t_c$ ) of 1087 s (Fig. 2a). In addition, the reaction mixture showed a clear EPR signal with  $g = 2.005$  and 1.4 mT peak-to-peak width (Fig. 2a, inset), reminiscent of the signals of porphyrin and chlorin radicals<sup>19,20</sup>. The signal suggests the formation of a Chl *c* anion radical, which probably has a smaller extinction coefficient in the visible range than a Chl *a* anion radical<sup>21</sup>. The  $g$  value higher than that of other porphyrin radicals may reflect geometric distortion due to the unique protein environment of the binding cavity, covered by the BchB C-terminal helix that is partly unwound by the binding of the substrate<sup>12</sup>. The broad EPR signal suggests a magnetic interaction with the spin on NB-cluster. Actually, fast spin relaxation of the Chl *c* radical was estimated based on the high values of microwave power at 7.6 mW required to half-saturate the signal intensity ( $P_{1/2}$ ) at 20 K and of inhomogeneity parameter ( $b$ ) of 1.46 (data not shown). In the class Ib ribonucleotide reductase of *Escherichia coli*, which contains a Tyr radical located at a short distance  $\sim 8$  Å from the metal binding site<sup>22</sup>, the high  $P_{1/2}$  value of the Tyr radical at 1.6 mW at 3.6 K was decreased to 0.03 mW when the ferromagnetic-coupling with a  $Mn^{III}Mn^{III}$  centre was relieved by the exchange of the centre to  $Fe^{III}Fe^{III}$  one with  $S = 0$ <sup>23</sup>. On the other hand, a Tyr radical in photosystem II exhibited a rather low  $P_{1/2}$  value of 60  $\mu$ W at 20 K<sup>24</sup> because its distance from the non-haem iron with  $S = 2$  is rather long at  $\sim 37$  Å<sup>25</sup>. Therefore, the high values of  $P_{1/2}$  and  $b$  above 1 indicate that the radical spin in the substrate binding site interacts with the NB-cluster with  $S = 3/2$ <sup>26</sup> at a short distance of  $\sim 10$  Å<sup>12</sup>.

No modification of chemical structure of Chl *c* seems to have occurred during this spectral change because given that Chl *c* was recovered with a high yield of 84% by acetone extraction after the reaction (Table S1). We accordingly suggest that the slow absorption decrease represents the formation of a Chl *c* anion radical by the one-electron reduction process, and that the electron transfer from the NB-cluster to Chl *c* occurs even though both proton transfer paths are blocked. The result also implies that the first step of the Pchl *d* reduction in the NB-protein includes the single electron transfer step from the NB-cluster to Pchl *d*.

In the WT-Chl *c* combination (Fig. 1d), the spectral change after the initiation of the reaction was less evident (Fig. 2b). It was smaller than that detected in the reaction of D274A-Chl *c*. A very weak EPR signal with  $g = 2.006$  was detected (data not shown) in accord with the smaller spectral change. The result suggested that the Chl *c* anion radical is also generated in this reaction. The lower amount of the Chl *c* anion radical may come from a lower level of bound Chl *c* to WT protein (approximately 25%) than that to D274A NB-protein. This result suggests that the Chl *c* anion radical is formed even when the putative proton donor for C18 is deleted.

The third combination, D274A-Pchl *d* (Fig. 1e), produced a marked spectral change immediately after the reaction start (Fig. 2c). In a first phase ( $< 400$  s), four absorption peaks at 451, 540, 583 and 632 nm, which represent the bound Pchl *d*, slowly decreased. The reaction mixture after 360 s showed a clear EPR signal with  $g = 2.004$  and a broad 1.7-mT bandwidth (Fig. 2c, inset). The saturation power  $P_{1/2}$  was also high at 8.9 mW and the factor  $b$  was estimated to be 1.30, as was the case with Chl *c*. The broader bandwidth than that of a putative Chl *c* anion radical may be attributed to larger hyperfine coupling, suggesting stronger or more complex hydrogen bonding to its binding cavity. The appearance of the EPR signal appeared to coincide with the bleaching of the Pchl *d* peaks, suggesting the formation of Pchl *d* radicals. In the absorption spectra, new peaks at 647, 659 and 707 nm appeared in a late phase ( $> 400$  s), suggesting that further reactions proceeded.

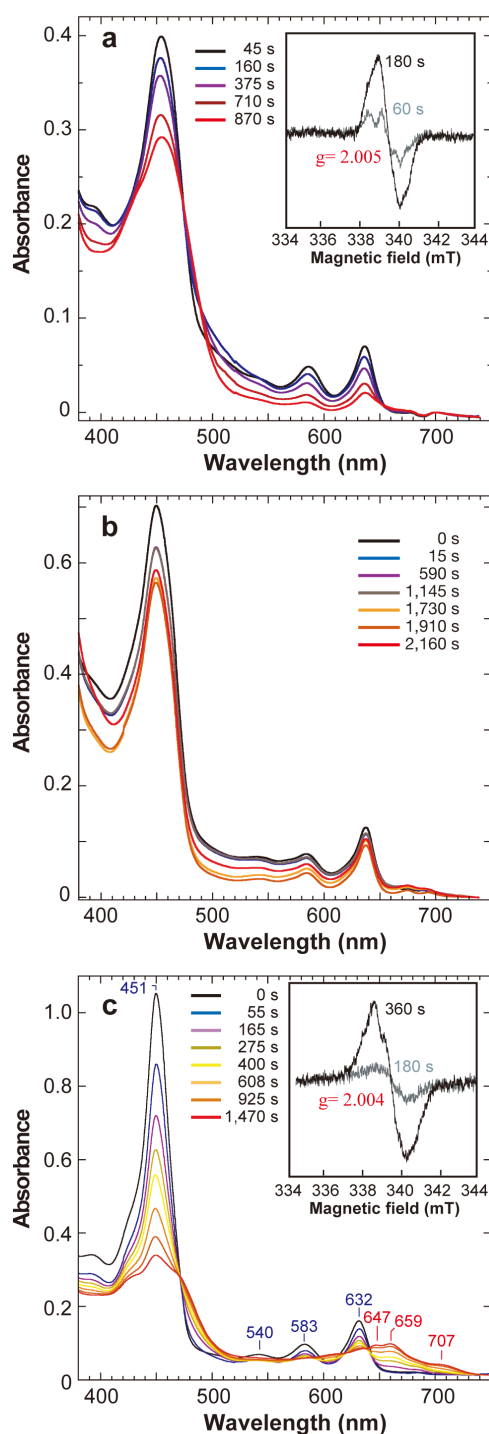


**Figure 2** | (a) Absorption spectra of the combination of D274A NB-protein and Chl *c*. Inset: EPR spectra of this combination. (b) Absorption spectra of the combination of WT NB-protein and Chl *c*. (c) Absorption spectra of the combination of D274A NB-protein and Pchl *d*. Inset: EPR spectra of this combination. All the absorption spectra were measured at 5 °C at varied times as shown in Figure after initiation of the reaction by adding ATP. EPR spectra were measured at 20 K after rapid freezing of the samples at times indicated in Figures as described in Methods. Note that the time courses are for the reaction at 5 °C and are expected to be significantly slower than those at physiological temperatures.

A global fitting analysis suggested that this spectral change could be decomposed into four independent components (Fig. 3a). The first component corresponds to the initial state (State 0; Fig. 2c, 0 s) of the D274A-NB-protein–Pchl *d* bound form (Fig. 3a, gray).

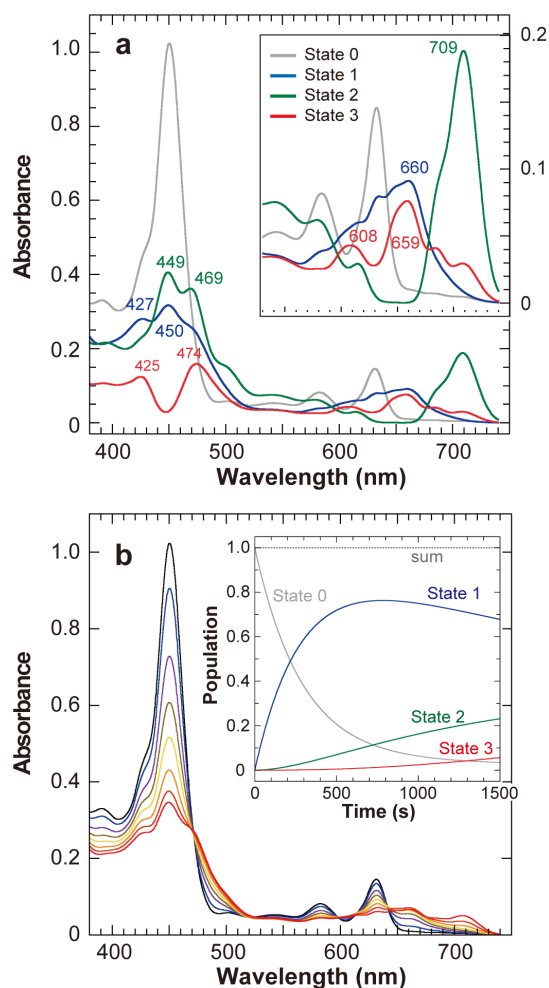


**Figure 3** | (a) Four absorption spectra (States 0 to 3) decomposed from those of Fig. 2c. State 0 is identical to that at 0 s in Fig. 2c. All spectra represent the states when the respective spectral component occupies 100%. Inset: A close up of the spectra of from 530 to 750 nm. (b) Simulated spectra by the four decomposed spectra. Inset: Time course of the population of the four spectral components.

Upon the initiation of the reaction, a second component (State 1) with three absorption peaks at 427, 450 and 660 nm grows with a  $t_c$  of 300 s (Fig. 3a, blue). Later, a third component (State 2) with peak at 449, 469 and 709 nm appears with a  $t_c$  of 3138 s (Fig. 3a, green), followed by a fourth component (State 3) with peak at 425, 474, 608 and 659 nm and a  $t_c$  of 2913 s (Fig. 3c, red). Although the shape of the decomposed spectra (Fig. 3a) still appears complex, suggesting that multiple intermediates are included in addition to the probable major intermediates, the simulated spectral changes fitted the observed ones very well (Figs. 2c and 3b).

To determine how the reactions proceeded in these combinations the pigments were extracted with acetone after the reactions (Table S1). In comparison with the high recovery of Chl *c* (69% and 84%), that of Pchlde was markedly low (32%) in D274A-Pchlde. Furthermore, a small amount of Chlide (2%) was detected in D274A-Pchlde. This indicated that a small portion of Pchlde proceeded further beyond the first radical formation step, even though the proton path to C17 was blocked. In contrast, no products were detected in the other two combinations (WT/Chl *c* and D274A/Chl *c*), suggesting that only the first electron transfer occurs and further reactions do not proceed once the proton path to C18 is blocked. Thus, the proton transfer event for C18 from the propionate may precede that for C17 from Asp274.

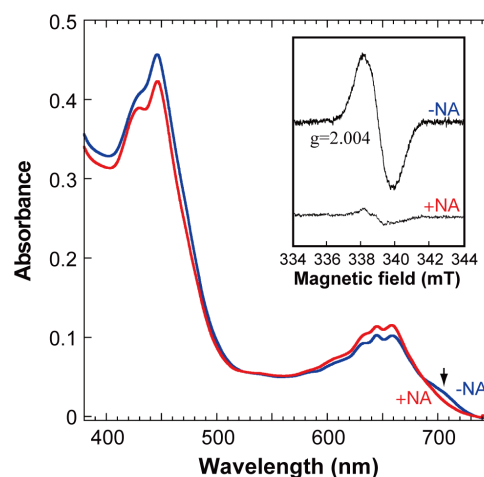


**Figure 4** | Absorption spectra of the combination of D274A and Pchlde in the presence (red) and absence (blue) of NA. An arrow indicates the decreased peak at 705 nm upon the NA addition. Inset: EPR spectra of the combination of D274A and Pchlde in the presence (lower trace) and absence (upper trace) of NA.

NA is a specific inhibitor of the electron transfer from L-protein to the NB-protein<sup>9</sup>. The Pchlde radicals detected in D274A-Pchlde appear to be in a steady state with respect to quenching and generation. Thus, upon NA addition, the electron transfer from the NB-cluster is blocked and unstable Pchlde radical species disappear in a short time. NA was added to the D274A-Pchlde reaction at the beginning of the late phase (420 s). The intensity of the EPR signal at  $g = 2.004$  decreased to approximately 20% of the control (Fig. 4, inset). This decrease of the EPR signal was accompanied by a significant change in the absorption spectra (Fig. 4). A characteristic shoulder at 705 nm disappeared, together with a significant decrease of peaks in the blue region, whereas the increase in the peaks near 650 nm was relatively slight. Pchlde radicals showing the  $g = 2.004$  signal may consist of at least two distinct molecular species, an NA-sensitive and an NA-insensitive species, under steady-state conditions. The concomitant decrease in the peak at 705 nm and the EPR signal ( $g = 2.004$ ) suggested that the NA-sensitive species represents State 2 with a 709-nm peak.

To serve as the first proton donor for C18, the C17-propionate must be protonated before the proton transfer. Considering that the probable  $pK_a$  of C17-propionic acid of Pchlde is similar to those of the free acids (propionic acid,  $pK_a = 4.87$ ; butyric acid,  $pK_a = 4.82$ ), the C17-propionate is deprotonated under the reaction conditions (pH 7.4). BchB-His378 located 6.5 Å from the propionate, is the best candidate for the proton donor (Fig. S2a). The C17-propionate may be protonated by His378 via a water molecule located 2.6 Å from the propionate. This probable contribution was supported by partial activity of a site-directed variant BchB-H378A (Fig. S2b), which is consistent with that of the equivalent site-directed variant H394A of *Prochlorococcus marinus* (35% activity)<sup>14</sup>. The distorted conformation of C17-propionate of Pchlde may contribute to the proton relay from His378 to the propionate via water molecules in the NB-protein (Fig. S2a).

## Discussion

We propose a reaction scheme in Figure 5 based on the results in the present study. In the model, the C17-propionate is already protonated (Fig. 5a, State 0) by proton transfer from His378 (Fig. S2a). The first step is the reduction of Pchlde by a single electron transfer from the NB-cluster, to form a Pchlde anion radical (Intermediate 1, Fig. 5b), which is based on the observation of Pchlde/Chl *c* radical formation in all three combinations. Following this, proton transfer

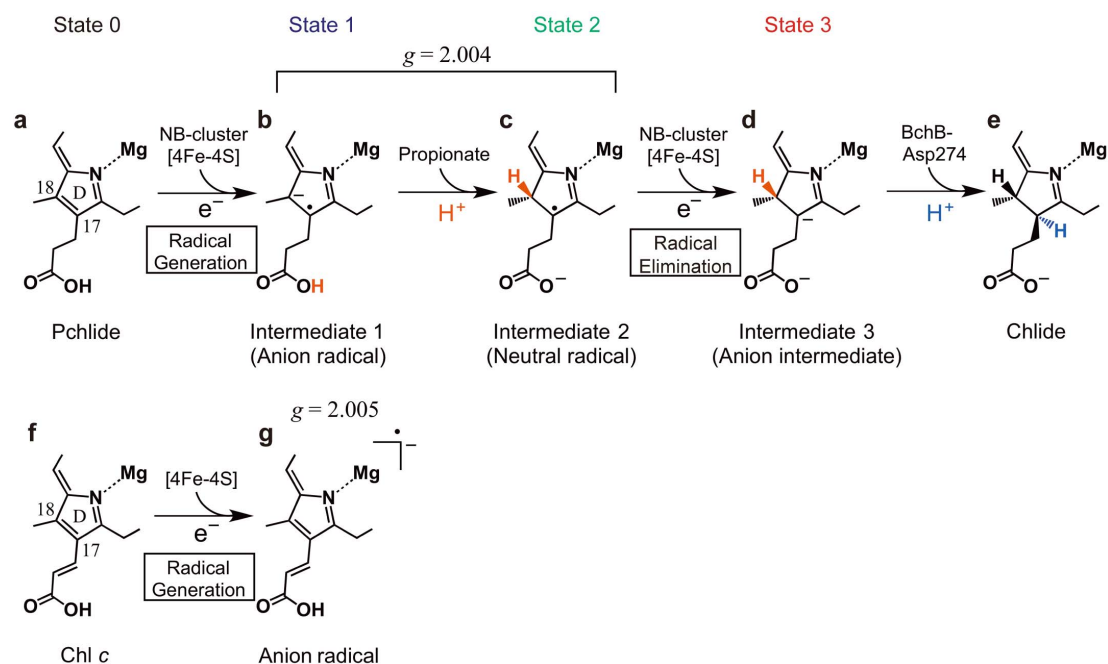


**Figure 5** | Proposed reaction steps in the Pchlide reduction (a–e). First step is the electron transfer from the NB-cluster to Pchlide (a) to form a Pchlide anion radical (b) followed by the proton transfer from the propionate to form a neutral radical (c). The second electron transfer eliminates the neutral radical by reduction to form an anion intermediate (d). The Pchlide reduction is completed by the second proton transfer (e). When Chl *c* is used instead of Pchlide (f), a Chl *c* anion radical is generated (g).

from the C17-propionate (shown in red) of Pchlide forms a second radical, a Pchlide neutral radical (Intermediate 2, Fig. 5c), which is based on the observation that no chemically altered products were detected in the combinations with Chl *c* and that a small amount of Chlide was detected in D274A/Pchlide. Both radicals are EPR active, and only a signal with the  $g$  value of 2.004 was detected (Fig. 2c, inset). Although we did not identify either of the two intermediates to represent the EPR signal, we propose that States 1 and 2 constitute the radical species. The coincident decrease of the EPR signal and the 705-nm shoulder of absorption spectra upon the NA addition (Fig. 4, inset) suggests that State 2 (with a 709-nm peak) is the NA-sensitive species. A second single electron transfer from the NB-cluster eliminates the radicals to form a non-radical anion (Intermediate 3, Fig. 5d) as State 3. The reaction is completed by the second proton transfer from Asp274 to form Chlide (Fig. 5e).

Crystallographic analysis of the complex of L-protein and NB-protein from *P. marinus* suggested that a water molecule just above C18 is the direct proton donor for C18 rather than the C17-propionate in the *Prochlorococcus* NB-protein<sup>14</sup>. However, contribution of the water molecule has not yet been experimentally proven to be critical for Pchlide reduction in the *Prochlorococcus* DPOR. Results we obtained so far in *R. capsulatus* DPOR support the reaction mechanism of the C17-propionate as the proton donor to C18.

The catalytic mechanism of the other Pchlide reductase, LPOR<sup>5</sup>, is completely different from that of DPOR. In a photoactive ternary complex of LPOR–NADPH–Pchlide, light absorption by the bound-Pchlide molecule creates a charge-transfer intermediate that triggers a hydride transfer from the NADPH-nicotinamide ring to the C17 carbon. Subsequently, a conserved Tyr residue donates a proton to the C18 carbon<sup>27</sup>. Although a first photochemical intermediate  $A_{696}$  was once assumed to be a Pchlide radical in initial works<sup>19</sup>,  $A_{696}$  was later regarded as a charge transfer complex generated by hydride transfer from NADPH by a detailed spectroscopic analysis<sup>20</sup>. Thus, the LPOR reaction does not appear to involve radical intermediates<sup>20</sup>. The catalytic steps of LPOR were dissected into one light-driven step and four light-independent steps by a ultrafast pump-probe absorp-

tion difference spectroscopy<sup>4</sup>. Further analyses suggest that a first photon absorption activates the LPOR–NADPH–Pchlide complex and a second photon absorption then induces catalysis<sup>4</sup>. Photosynthetic organisms, thus, have found two distinct solutions to catalyse the Pchlide reduction using totally different protein architectures, nitrogenase and SDR, during evolution<sup>2</sup>.

Nitrogenase shares a common architecture with DPOR<sup>12</sup>. The overall reaction involves transfers of eight electrons and eight protons to produce ammonia and hydrogen, consisting of at least 10 reaction intermediates<sup>28</sup>. Efforts to trap reaction intermediates lead to characterization of an important intermediate state E4 that carries four electrons stored as two [Fe–H–Fe] bridging hydrides and two protons bound to the sulfides on the FeMo-cofactor<sup>28,29</sup>. The currently proposed reaction scheme that predicts the E4 state suggests that the coupling between electron and proton transfers is too tight to be discriminated. In contrast, we succeeded to identify the sequential electron and proton transfer steps on the NB-protein in the DPOR reaction, by blocking of the proton transfer step using D274A and Chl *c*. It is of interest that the two types of reaction mechanisms in DPOR and nitrogenase seem to have diverged from the common structural architectures during evolution.

In terms of reaction mechanism, DPOR appears to be similar to some radical enzymes rather than nitrogenase. Crystal structure of 2HCD<sup>30</sup> suggested that one of the two [4Fe–4S] clusters in the heterodimeric structure transfers one electron to the substrate to generate a ketyl radical followed by dehydration of 2-hydroxy group with the  $\beta$ -proton. Then, the radical is eliminated by electron transfer back to the [4Fe–4S] cluster (oxidation). In DPOR, the Pchlide radical is generated by the electron transfer from the NB-cluster similar to 2HCD (Figs. 5a–b). However, the Pchlide radical is eliminated by a second electron transfer (reduction), followed by the proton transfer to produce the final product, Chlide (Figs. 5c–e). Benzoyl-CoA reductase (BCR) may adopt the reaction mechanism more similar to that of DPOR. BCR catalyses two-electron reduction of benzoyl-CoA with two-proton transfer to form stereo-selectively *trans*-dienoyl-CoA product<sup>31</sup>, and this enzyme carries two [4Fe–4S]



clusters that may act as the radical generator to catalyse the reduction<sup>32</sup>. Comparison of the reaction mechanism based on crystal structure of BCR would be very interesting.

**Phycocyanobilin:ferredoxin oxidoreductase PcyA**, which catalyses two vinyl reductions of biliverdin IX $\alpha$  in bilin biosynthesis, is the other example of an enzyme that generates substrate radicals during catalysis<sup>33,34</sup>. Substrate bilin radicals are generated by electron transfer from a small FeS protein, ferredoxin. The reaction involves sequential electron-coupled proton transfers. PcyA does not carry any metal ions or cofactors, but ferredoxin plays a role as the electron donor. DPOR is distinct from PcyA in that the direct electron donor, the NB-cluster, is embedded in the NB-protein.

Radical-mediated Pchl $\text{d}$  reduction by DPOR functions very efficiently under anaerobic conditions. However, such a reaction is potentially dangerous under oxygen-rich conditions because the substrate radical would be a source of reactive oxygen species that would cause severe damage to cells<sup>35</sup>. In fact, another nitrogenase-like enzyme Chl $\text{d}$  oxidoreductase<sup>36</sup>, a close relative of DPOR, becomes a superoxide-generator in the photosynthetic bacterium *R. sphaeroides* and *Synechocystis* sp. PCC 6803<sup>37,38</sup>. Nevertheless DPOR is distributed widely among oxygenic photosynthetic organisms including cyanobacteria, green algae, bryophytes, pteridophytes and gymnosperms (Figs. S3 and S4). As observed in green dark-grown seedlings of some gymnosperms<sup>39–41</sup>, the Pchl $\text{d}$ -radical mediated reaction plays a critical role in the greening of many photosynthetic organisms inhabiting light-limited environments.

## Methods

**Protein purification.** All manipulations were performed in an anaerobic chamber<sup>7</sup>. WT, D274A and H378A NB-protein variants were overexpressed in *E. coli* harbouring pHANB1<sup>42</sup>, pJnD274A (this plasmid was used for the preparation of D274A variant in the previous report)<sup>12</sup> and pJnH378A (see below), respectively. NB-protein was purified from crude extracts on a Strep-Tactin (IBA) affinity chromatography column equilibrated with 100 mM Tris-HCl (pH 8.0) containing 150 mM NaCl and eluted with 100 mM Tris-HCl (pH 8.0) containing 150 mM NaCl and 2.5 mM desthiobiotin. Pchl $\text{d}$ - or Chl  $c$ -bound forms of WT and D274A were prepared as described previously<sup>7</sup>. The molar ratio of Pchl $\text{d}$  in the obtained WT or D274A variant NB-protein is 1.1–1.2 and that of Chl  $c$  in WT or D274A variant NB-protein is 0.3 or 0.9–1.0, respectively.

**Site-directed mutagenesis.** Nucleotide substitutions causing amino acid change were introduced into *bchB* region of pHANB1<sup>42</sup> using two primers, BchBH378Ala-f1 (5'-ggtgatAtcggcgccctcGCGgtgcaggacttcccgccc-3') and BchBH378Ala-r1 (5'-cgggcggggaagtctctgcacCCGcgacggcgccgaTatcacc-3'). The changed nucleotides are shown in upper case and the codons corresponding to the amino acid residues to be changed are capitalised and underlined. To easily confirm the introduction of the mutations, another silent mutation besides the targeted codon was introduced to create a new restriction site (EcoRV). PCR reactions were performed with KOD-plus polymerase (Toyobo, Osaka, Japan). The nucleotide sequences of mutagenised *bchB* were confirmed by DNA sequencing.

**Absorption spectral measurements.** To monitor the change in absorption spectra of the DPOR reaction mixture, the assay pre-mixture was prepared in a cuvette with an airtight screw cap in an anaerobic chamber. After incubation of Pchl $\text{d}$ - or Chl  $c$ -bound NB-protein (5  $\mu\text{M}$ ) with L-protein (10  $\mu\text{M}$ ), creatine phosphate (20 mM), creatine phosphokinase (21 units) and sodium dithionite (2.7 mM) in 100 mM HEPES-KOH (pH 8.0) for 10 min at 5°C, a pre-chilled mixture of ATP and MgCl<sub>2</sub> (final concentration 9 mM and 5 mM, respectively) was added using a syringe and absorption spectra were periodically recorded with a Jasco V550 spectrophotometer (Jasco, Hachioji, Japan) having a temperature control module (model ETC-477, set at 5°C; Jasco). To determine the amount of recovered of pigments, the assay mixture was mixed with acetone (final concentration 80%) and absorption spectra were recorded with a Jasco V550 spectrophotometer.

**Preparation of EPR samples.** For EPR spectroscopy, the DPOR assay pre-mixtures were prepared in quartz EPR tubes (outer diameter 5 mm) in the anaerobic chamber. Pchl $\text{d}$ - or Chl  $c$ -bound NB-protein (10  $\mu\text{M}$ ) was incubated for 10 min at 3°C with L-protein (20  $\mu\text{M}$ ), creatine phosphate (20 mM), creatine phosphokinase (21 units) and sodium dithionite (2.7 mM) in 100 mM HEPES-KOH (pH 8.0). After capping, a pre-chilled mixture of ATP and MgCl<sub>2</sub> (final concentration 9 mM and 5 mM, respectively; prepared and packed in an anaerobic chamber) was added to the tube using a syringe outside the anaerobic chamber. After mixing ATP and MgCl<sub>2</sub>, the reaction mixtures were incubated for 6 min at 3°C and frozen rapidly in liquid nitrogen to quench the reaction and EPR spectra were recorded. EPR measurements were performed using a Bruker ESP-300E X-band spectrometer (Bruker Biospin,

Germany) equipped with a liquid-helium flow cryostat and a temperature control system (CF935, Oxford Instruments, UK). Experimental conditions were as follows: microwave frequency, 9.507–9.563 GHz; modulation frequency, 100 kHz; temperature, 20 K; modulation amplitude, 0.4 mT; and time constant, 20 ms.

**NA inhibition.** After the addition of ATP and MgCl<sub>2</sub>, the reaction mixtures of D274A/Pchl $\text{d}$  were incubated for 7 min at 5°C and NA was subsequently added (70 mM). After additional incubation for 3 min, absorption spectra were recorded. For EPR spectroscopy, the reaction mixtures were frozen rapidly in liquid nitrogen and EPR spectra were recorded. For the control (–NA), only the buffer (100 mM HEPES-KOH; pH 8.0) was added and spectrum were recorded.

**Global fitting procedure.** The absorption spectra at each time (Fig. 2c) were decomposed into 20 Gaussian bands. The band positions were determined from the second-derivative spectra and the band widths by a global multi-Gaussian fitting analysis. The amplitudes of each band were plotted against time. The time courses were analysed with a global fitting using a rate equation between 4 states, in which the spectra for States 0, 2 and 3 were assumed to be the 0-s spectrum (Fig. 2c), the differential spectra between the presence and absence of NA (Fig. 4) and between the 0-s and 1470-s spectra (Fig. 2c), respectively. The time constants for forward and backward reactions were restricted to 10–5000 s and 10–10000 s, respectively. Absorption spectral changes (Fig. 3b) were reconstructed with the spectra and population changes of each state.

- Masuda, T. & Takamiya, K. Novel insights into the enzymology, regulation and physiological functions of light-dependent protochlorophyllide oxidoreductase in Angiosperms. *Photosynth. Res.* **81**, 1–29 (2004).
- Reinbothe, C. *et al.* Chlorophyll biosynthesis: spotlight on protochlorophyllide reduction. *Trends Plant Sci.* **15**, 614–622 (2010).
- Heyes, D., Ruban, A., Wilks, H. & Hunter, C. Enzymology below 200 K: the kinetics and thermodynamics of the photochemistry catalyzed by protochlorophyllide oxidoreductase. *Proc. Natl. Acad. Sci. USA* **99**, 11145–11150 (2002).
- Sytina, O. *et al.* Conformational changes in an ultrafast light-driven enzyme determine catalytic activity. *Nature* **456**, 1001–1004 (2008).
- Heyes, D. & Hunter, C. Making light work of enzyme catalysis: protochlorophyllide oxidoreductase. *Trends Biochem. Sci.* **30**, 642–649 (2005).
- Nomata, J., Kitashima, M., Inoue, K. & Fujita, Y. Nitrogenase Fe protein-like Fe-S cluster is conserved in L-protein (BchL) of dark-operative protochlorophyllide reductase from *Rhodobacter capsulatus*. *FEBS Lett* **580**, 6151–6154 (2006).
- Nomata, J., Ogawa, T., Kitashima, M., Inoue, K. & Fujita, Y. NB-protein (BchN-BchB) of dark-operative protochlorophyllide reductase is the catalytic component containing oxygen-tolerant Fe-S clusters. *FEBS Lett.* **582**, 1346–1350 (2008).
- Bröcker, M. *et al.* Biosynthesis of (bacterio)chlorophylls: ATP-dependent transient subunit interaction and electron transfer of dark-operative protochlorophyllide oxidoreductase. *J. Biol. Chem.* **285**, 8268–8277 (2010).
- Nomata, J., Kondo, T., Itoh, S. & Fujita, Y. Nicotinamide is a specific inhibitor of dark-operative protochlorophyllide oxidoreductase, a nitrogenase-like enzyme, from *Rhodobacter capsulatus*. *FEBS Lett.* **587**, 3142–3147 (2013).
- Nomata, J., Swem, L., Bauer, C. & Fujita, Y. Overexpression and characterization of dark-operative protochlorophyllide reductase from *Rhodobacter capsulatus*. *Biochim. Biophys. Acta* **1708**, 229–237 (2005).
- Sarma, R. *et al.* Crystal structure of the L protein of *Rhodobacter sphaeroides* light-independent protochlorophyllide reductase with MgADP bound: a homologue of the nitrogenase Fe protein. *Biochemistry* **47**, 13004–13015 (2008).
- Muraki, N. *et al.* X-ray crystal structure of the light-independent protochlorophyllide reductase. *Nature* **465**, 110–114 (2010).
- Bröcker, M. J. *et al.* Crystal structure of the nitrogenase-like dark operative protochlorophyllide oxidoreductase catalytic complex (ChlN/ChlB)<sub>2</sub>. *J. Biol. Chem.* **285**, 27336–27345 (2010).
- Moser, J. *et al.* Structure of ADP-aluminium fluoride-stabilized protochlorophyllide oxidoreductase complex. *Proc. Natl. Acad. Sci. USA.* **110**, 2094–2098 (2013).
- Nordlund, P. & Reichard, P. Ribonucleotide reductases. *Annu. Rev. Biochem.* **75**, 681–706 (2006).
- Dowling, D. P., Croft, A. K. & Drennan, C. L. Radical use of Rossmann and TIM barrel architectures for controlling coenzyme B<sub>12</sub> chemistry. *Annu. Rev. Biophys.* **41**, 403–427 (2012).
- Shisler, K. A. & Broderick, J. B. Emerging themes in radical SAM chemistry. *Curr. Opin. Struct. Biol.* **22**, 701–710 (2012).
- Kim, J., Darley, D. J., Buckel, W. & Pierik, A. J. An allylic ketyl radical intermediate in clostridial amino-acid fermentation. *Nature* **452**, 239–242 (2008).
- Lebedev, N. & Timko, M. Protochlorophyllide oxidoreductase B-catalyzed protochlorophyllide photoreduction in vitro: insight into the mechanism of chlorophyll formation in light-adapted plants. *Proc. Natl. Acad. Sci. USA* **96**, 9954–9959 (1999).
- Heyes, D. *et al.* The first catalytic step of the light-driven enzyme protochlorophyllide oxidoreductase proceeds via a charge transfer complex. *J. Biol. Chem.* **281**, 26847–26853 (2006).



21. Fujita, I., Davis, M. S. & Fajer, J. Anion radicals of pheophytin and chlorophyll *a*: their role in the primary charge separations of plant photosynthesis. *J. Am. Chem. Soc.* **100**, 6280–6282 (1978).
22. Cox, N. *et al.* A tyrosyl-dimanganese coupled spin system is the native metalloradical cofactor of the R2F subunit of the ribonucleotide reductase of *Corynebacterium ammoniagenes*. *J. Am. Chem. Soc.* **132**, 11197–11213 (2010).
23. Cotruvo, J. A. & Stubbe, J. An active dimanganese(III)-tyrosyl radical cofactor in *Escherichia coli* class Ib ribonucleotide reductase. *Biochemistry* **49**, 1297–1309 (2010).
24. Isogai, Y., Nishimura, M. & Itoh, S. Charge distribution on the membrane surface of the donor side of photosystem II. Effect of the free radical relaxing agent dysprosium on the power saturation of EPR signal IIs in PS-II particles. *Plant Cell Physiol.* **28**, 1493–1499 (1987).
25. Hirsh, D. J., Beck, W. F., Innes, J. B. & Brudvig, G. W. Using saturation-recovery EPR to measure distances in proteins: applications to photosystem II. *Biochemistry* **31**, 532–541 (1992).
26. Kondo, T., Nomata, J., Fujita, Y. & Itoh, S. EPR study of 1Aps-3Cys ligated 4Fe-4S iron-sulfur cluster in NB-protein (BchN-BchB) of a dark-operative protochlorophyllide reductase complex. *FEBS Lett.* **585**, 214–218 (2011).
27. Wilks, H. & Timko, M. A light-dependent complementation system for analysis of NADPH:protochlorophyllide oxidoreductase: identification and mutagenesis of two conserved residues that are essential for enzyme activity. *Proc. Natl. Acad. Sci. USA* **92**, 724–728 (1995).
28. Hoffman, B. M., Lukoyanov, D., Dean, D. R. & Seefeldt, L. C. Nitrogenase: a draft mechanism. *Acc. Chem. Res.* **46**, 587–595 (2013).
29. Lukoyanov, D., Barney, B. M., Dean, D. R., Seefeldt, L. C. & Hoffman, B. M. Connecting nitrogenase intermediates with the kinetic scheme for N<sub>2</sub> reduction by a relaxation protocol and identification of the N<sub>2</sub> binding state. *Proc. Natl. Acad. Sci. USA* **104**, 1451–1455 (2007).
30. Knauer, S. H., Buckel, W. & Dobbek, H. Structural basis for reductive radical formation and electron recycling in (*R*)-2-hydroxyisocaproyl-CoA dehydratase. *J. Am. Chem. Soc.* **133**, 4342–4347 (2011).
31. Thiele, B., Rieder, O., Golding, B. T., Müller, M. & Boll, M. Mechanism of enzymatic Birch reduction: stereochemical course and exchange reactions of benzoyl-CoA reductase. *J. Am. Chem. Soc.* **130**, 14050–14051 (2008).
32. Unciuleac, M. & Boll, M. Mechanism of ATP-driven electron transfer catalyzed by the benzene ring-reducing enzyme benzoyl-CoA reductase. *Proc. Natl. Acad. Sci. USA* **98**, 13619–13624 (2001).
33. Tu, S. L., Rockwell, N. C., Lagarias, J. C. & Fisher, A. J. Insight into the radical mechanism of phycocyanobilin-ferredoxin oxidoreductase (PcyA) revealed by X-ray crystallography and biochemical measurements. *Biochemistry* **46**, 1484–1494 (2007).
34. Stoll, S. *et al.* Structure of the biliverdin radical intermediate in phycocyanobilin:ferredoxin oxidoreductase identified by high-field EPR and DFT. *J. Am. Chem. Soc.* **131**, 1986–1995 (2009).
35. Imlay, J. A. Iron-sulphur clusters and the problem with oxygen. *Mol. Microbiol.* **59**, 1073–1082 (2006).
36. Nomata, J., Mizoguchi, T., Tamiaki, H. & Fujita, Y. A second nitrogenase-like enzyme for bacteriochlorophyll biosynthesis - Reconstitution of chlorophyllide *a* reductase with purified X-protein (BchX) and YZ-protein (BchY-BchZ) from *Rhodobacter capsulatus*. *J. Biol. Chem.* **281**, 15021–15028 (2006).
37. Kim, E. J., Kim, J. S., Lee, I. H., Rhee, H. J. & Lee, J. K. Superoxide generation by chlorophyllide *a* reductase of *Rhodobacter sphaeroides*. *J. Biol. Chem.* **283**, 3718–3730 (2008).
38. Kim, E. J., Kim, J. S., Rhee, H. J. & Lee, J. K. Growth arrest of *Synechocystis* sp. PCC6803 by superoxide generated from heterologously expressed *Rhodobacter sphaeroides* chlorophyllide *a* reductase. *FEBS Lett.* **583**, 219–223 (2009).
39. Kusumi, J., Sato, A., Tachida, H. & Investigators, S. T.-N. Y. Proceedings of the SMBE Tri-National Young Investigators' Workshop 2005. Relaxation of functional constraint on light-independent protochlorophyllide oxidoreductase in *Thuja*. *Mol. Biol. Evol.* **23**, 941–948 (2006).
40. Demko, V. *et al.* A novel insight into the regulation of light-independent chlorophyll biosynthesis in *Larix decidua* and *Picea abies* seedlings. *Planta* **230**, 165–176 (2009).
41. Yamamoto, H., Kurumiya, S., Ohashi, R. & Fujita, Y. Functional evaluation of a nitrogenase-like protochlorophyllide reductase encoded by the chloroplast DNA of *Physcomitrella patens* in the cyanobacterium *Leptolyngbya boryana*. *Plant Cell Physiol.* **52**, 1983–1993 (2011).
42. Yamamoto, H., Nomata, J. & Fujita, Y. Functional expression of nitrogenase-like protochlorophyllide reductase from *Rhodobacter capsulatus* in *Escherichia coli*. *Photochem. Photobiol. Sci.* **7**, 1238–1242 (2008).

## Acknowledgments

We thank Wolfgang Buckel, Kazuyuki Tatsumi, Tatsuo Omata and Kazuki Terauchi for the valuable discussion. This study was supported by Grants-in-Aid for Scientific research Nos 20200063, 23370020, 23000007 (Y.F.) and 22245030 (H.T.) from the Japan Society for the Promotion of Science (JSPS), by the Precursory Research for Embryonic Science and Technology (PRESTO), and by the Advanced Low Carbon Technology Research and Development Program (ALCA) of the Japan Science and Technology Agency (JST). T.K. is also grateful for a Fellowship from the JSPS for Japanese Junior Scientists (24008402).

## Author contributions

J.N. purified NB-proteins and performed site-directed mutagenesis, enzymatic assay and absorption spectroscopy; T.K., S.I. and J.N. performed EPR spectroscopy; T.M. and H.T. prepared Chl *c*; Y.F., J.N. and S.I. contributed to design of the experiments and writing the manuscript. All authors discussed the results and commented on the manuscript.

## Additional information

**Supplementary information** accompanies this paper at <http://www.nature.com/scientificreports>

**Competing financial interests:** The authors declare no competing financial interests.

**How to cite this article:** Nomata, J. *et al.* Dark-operative protochlorophyllide oxidoreductase generates substrate radicals by an iron-sulphur cluster in bacteriochlorophyll biosynthesis. *Sci. Rep.* **4**, 5455; DOI:10.1038/srep05455 (2014).



This work is licensed under a Creative Commons Attribution-NonCommercial-ShareAlike 4.0 International License. The images or other third party material in this article are included in the article's Creative Commons license, unless indicated otherwise in the credit line; if the material is not included under the Creative Commons license, users will need to obtain permission from the license holder in order to reproduce the material. To view a copy of this license, visit <http://creativecommons.org/licenses/by-nc-sa/4.0/>